Self-Energy Concept for the Numerical Solution of the Liouville-von Neumann Equation

Khuram Shahzad Khalid, Lukas Schulz [ID], and Dirk Schulz

Abstract—A new numerical approach is presented for the determination of the statistical density matrix as a solution of the Liouville-von Neumann equation in center-mass coordinates. The numerical discretization is performed by utilizing a finite volume method, which leads to a discretized drift and diffusion operator. The solution is based on the eigenvector basis of the discretized diffusion operator with its corresponding eigenvalues and on the introduction of the self-energy concept. More specifically, the self-energy concept is essential to describe open-boundary problems adequately. Furthermore, this approach allows the definition of inflow and outflow conditions. The method presented is investigated with regard to the conventional Wigner transport equation and the quantum transmitting boundary method, when investigating coherent effects.

Index Terms—Liouville-von Neumann equation, quantum transmitting boundary method, resonant tunneling diode, statistical density matrix, Wigner transport equation.

I. INTRODUCTION

RECENT progress in the field of nanoelectronics technology drives the device dimensions towards space and time scales where the application of quantum approaches for the solution of carrier transport equations are primarily important. Numerous approaches have been investigated in the past for the determination of carrier transport equations [1], for instance either utilizing coherent models based on the solution of the Schrödinger equation [2] or kinetic models conventionally applying the Wigner-Weyl transform [3]–[5] or non-equilibrium Green's function approaches [6], [7]. Most importantly in the past few decades, the analysis of carrier transport in quantum devices is performed by the Wigner function formalism using conventional finite difference schemes such as upwind difference schemes [8],[9] or hybrid difference schemes [10]. But, the use of these finite difference schemes leads to several drawbacks. Firstly, the overestimation of the diffusion current by using upwind difference or hybrid difference schemes results in an incorrect description of coherence effects [11]. Secondly, the non-local kinetic operator is not correctly incorporated and linked with the boundary conditions [12]. This results in an

incorrect description of coherence effects. These drawbacks can be avoided by using an approximation of the phase space operator as proposed in [13]. Furthermore, another major drawback is caused by the numerical approximation of the drift operator, when a discrete Wigner-Weyl transform is applied onto the statistical density matrix. As a consequence, a discrete convolution operation between the statistical density matrix and the drift operator appears within the quantum Liouville-von Neumann equation. The application of a discrete Fourier transform onto the drift term leads to the incorporation of high spatial frequencies in the Fourier series, particularly when external voltages are applied. The latter aspect results in numerical problems with respect to the diffusion operator [14].

In literature [15]–[17], the use of the Liouville-von Neumann equation has been formerly discussed without the use of center-mass coordinates, but the appearing system matrices are singular and, therefore, the solution is combined with numerical problems. To overcome these limitations, a new approach on the basis of the Liouville-von Neumann equation in center-mass coordinates is proposed and investigated. To allow a stringent presentation of the approach, a constant effective mass is assumed. Of course, the proposed approach can be reformulated to consider a position-dependent effective mass by applying a concept as described in [18]. The present contribution is organized as follows: At first, the numerical approximation of the Liouville-von Neumann equation in center-mass coordinates on the basis of a finite volume technique is discussed in Section II. Section III addresses the aspect, in which the Liouville-von Neumann equation can be solved in combination with the Poisson equation. In Section IV the statistical density matrix is calculated and evaluated for the equilibrium and the non-equilibrium case while investigating a resonant tunneling diode. The contribution ends with a final discussion of the results obtained followed by a conclusion in Section V.

II. DISCRETIZATION OF THE LIOUVILLE-VON NEUMANN EQUATION

A. Introduction of the Liouville-von Neumann Equation

The statistical density matrix describes a quantum system with a statistical ensemble of the eigenstates. The time evolution of the statistical density matrix is described by the Liouville-von Neumann equation

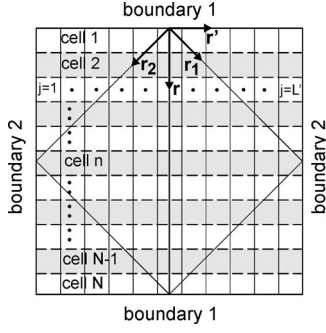$$\frac{\partial \rho}{\partial t} = \frac{\mathcal{L}}{i\hbar}\rho, \tag{1}$$

Fig. 1. Schematic picture of the computational domain with related center-mass coordinates r and r'. Cells defined by the parameter n are introduced in r-direction and defined by the parameter j in r'-direction, respectively.

where ρ represents the statistical density matrix and the Liouville-von Neumann operator can be expressed as

$$\mathcal{L} = \frac{\hbar^2}{2m}\left(\frac{\partial^2}{\partial r_2^2} - \frac{\partial^2}{\partial r_1^2}\right) + [V(r_1) - V(r_2)] \qquad (2)$$

assuming a constant effective mass distribution m. A voltage distribution Ψ is assumed and linked with the potential V by the definition $V = -e\Psi$, where e is the electron charge. The potential V includes the barrier potential, the Hartree-Fock potential and the potential due to the applied voltage. A coordinate transformation is applied by utilizing the relations

$$r = \frac{r_1 + r_2}{2} \text{ and } r' = r_1 - r_2, \qquad (3)$$

where r and r' represent the so called center-mass coordinates as shown in Fig. 1. Considering the stationary case and utilizing the coordinate transformation (3), (1) can be rewritten according to

$$i\frac{\hbar}{m}\frac{\partial}{\partial r}\frac{\partial}{\partial r'}\rho + i\frac{e}{\hbar}\left[\Psi\left(r + \frac{1}{2}r'\right) - \Psi\left(r - \frac{1}{2}r'\right)\right]\rho = 0. \qquad (4)$$

This is the transformed Liouville-von Neumann equation for center-mass coordinates [9]. The first term represents the diffusion term and the second term represents the drift term, respectively.

B. Discretization Utilizing the Finite Volume Technique

A standard finite volume scheme is applied for the numerical approximation of the transformed Liouville-von Neumann equation (4). For this purpose, the computational domain is divided into N cells with respect to the r-direction as depicted in Fig. 1. Accordingly, the discretization scheme with regard to the r'-direction is discussed at first. The derivations of the discretization matrices are discussed for each cell n. When starting with the discretization of the diffusion term and using L' discretization points in r'-direction, the relation

$$\frac{\partial}{\partial r'}\rho\big|_{r_j'} \cong \frac{\rho_{j+1}(r) - \rho_{j-1}(r)}{2 \cdot \Delta r'}, \qquad (5)$$

holds for each discrete location r_j' with $j = 1, ..., L'$. $\Delta r'$ is the discretization width in r'-direction and ρ_j represents the value of the density matrix ρ at the location r_j' but still depends on the

r-direction. Next, the drift term in (4) at each discrete location r_j' is approximated utilizing

$$\Delta\Psi_j(r) = \Psi\left(r + \frac{1}{2}r_j'\right) - \Psi\left(r - \frac{1}{2}r_j'\right). \qquad (6)$$

With these definitions, the diffusion and drift operator are approximated. A matrix $[A]_n$ describing the diffusion characteristics of the carriers in each cell n is introduced according to

$$[A]_n = \alpha \cdot \begin{bmatrix} a_{j,j-1} & a_{j,j} & a_{j,j+1} \end{bmatrix}, \qquad (7)$$

where α is given by $\alpha = i \cdot \hbar/(2 \cdot \Delta r' \cdot m)$ with $j \in 1, 2, \ldots, L'$. The values of the matrix elements are $a_{j,j-1} = -1$, $a_{j,j} = 0$ and $a_{j,j+1} = +1$. Similarly, a matrix $[B(r)]_n$ describing the drift behavior of the carriers is introduced, which represents a tridiagonal Toeplitz matrix given by

$$[B(r)]_n = \beta \cdot \begin{bmatrix} b_{j,j-1} & b_{j,j} & b_{j,j+1} \end{bmatrix}, \qquad (8)$$

with $\beta = -i \cdot e/(4 \cdot \hbar)$ and $j \in 1, 2, \ldots, L'$. The values of the matrix elements are $b_{j,j-1} = \Delta\Psi_j(r)$, $b_{j,j} = \Delta\Psi_j(r) + \Delta\Psi_{j+1}(r)$ and $b_{j,j+1} = \Delta\Psi_{j+1}(r)$. The values ρ_0 and $\rho_{L'+1}$ are located outside of the computational window at the boundary 2 as indicated in Fig. 1, so boundary conditions have to be introduced. We are following a concept, which is related to the self-energy concept. The main purpose of this concept is to describe the interaction between the physical behavior inside and outside of the computational window via open boundary conditions, so that the carrier injection as well as the carrier extraction between both spaces can be described. The latter aspect requires the introduction of inflow and outflow waves. For further details we refer to [19], [20]. Following the self-energy concept, the values ρ_0 and $\rho_{L'+1}$ at the boundary are expressed for each cell n dependent on interior values next to the boundary of the computational window by introducing self energies $\Sigma_{n,1}$ and $\Sigma_{n,L'}$ with respect to each cell. Finally, we arrive at

$$\rho_0 = \Sigma_{n,1} \cdot \rho_1 \quad \text{and} \quad \rho_{L'+1} = \Sigma_{n,L'} \cdot \rho_{L'}. \qquad (9)$$

With these definitions, the matrix elements $[A]_{1,1}$ and $[A]_{L',L'}$ have to be modified for each cell n according to

$$[A]_{1,1} = \Sigma_{n,1} \cdot a_{1,0} \quad \text{and} \quad [A]_{L',L'} = \Sigma_{n,L'} \cdot a_{L',L'+1}. \qquad (10)$$

Similarly, the matrix elements $[B]_{1,1}$ and $[B]_{L',L'}$ have to be replaced for each cell n by introducing the values

$$[B]_{1,1} = \Sigma_{n,1} \cdot b_{1,0} - b_{1,1} \qquad (11)$$

and

$$[B]_{L',L'} = \Sigma_{n,L'} \cdot b_{L',L'+1} - b_{L',L'} \qquad (12)$$

The choice of the self-energies $\Sigma_{n,1}$ and $\Sigma_{n,L'}$ will be discussed in Section II-D. The parameters $a_{1,0}, a_{L',L'+1}, b_{1,0}$ and $b_{L',L'+1}$ are defined by the matrix elements of the matrices $[A]_n$ and $[B]_n$ according to (7) and (8). The diffusion matrix $[A]_n$ and the drift matrix $[B(r)]_n$ are of the order $L' \times L'$. After summarizing all equations for each cell n we arrive at a matrix-vector equation

$$[A]_n \cdot \frac{\partial}{\partial r}\vec{\rho}(r) - [B(r)]_n \cdot \vec{\rho}(r) = \vec{0}. \qquad (13)$$

The matrix-vector equation (13) represents a system of ordinary coupled differential equations. In each cell n the matrix $[B(r)]_n$ is approximated by choosing the mean value of $\Delta\Psi_j(r_n)$ and $\Delta\Psi_j(r_{n-1})$ for the approximation of $\Delta\Psi_j(r)$. For each cell n the matrix $[B(r)]_n$ is replaced by a matrix $[B(r_n)]_n$ with constant entries. Hence, (13) can be rearranged for each cell n arriving at

$$[A]_n \cdot \frac{\partial}{\partial r}\vec{\rho}(r) = [B(r_n)]_n \cdot \vec{\rho}(r). \qquad (14)$$

C. Definition of Inflow and Outflow Waves

Up to this stage, a matrix-vector equation for each local cell n has been derived. Now, we are introducing the concept of "inflow" and "outflow" waves, as is the case for the Wigner transport equation [13]. For this purpose, the matrix $[A]_n$ in (14) is diagonalized by using a transformation to principal axis. A transformation matrix $[Q]_n$ consisting of the eigenvectors $\vec{q}_l$ of the matrix $[A]_n$ can be introduced. The eigenvectors $\vec{q}_l$ are placed in each row of the matrix $[Q]_n$ resulting in

$$[Q]_n = [\vec{q}_1, \vec{q}_2, \dots, \vec{q}_l, \dots, \vec{q}_{L'}]. \qquad (15)$$

With the use of the transformation matrix $[Q]_n$ the matrix $[A]_n$ is diagonalized according to

$$[Q]_n^{-1} \cdot [A]_n \cdot [Q]_n = [\Lambda]_n. \qquad (16)$$

The diagonal matrix $[\Lambda]_n$ includes the eigenvalues λ_l of the matrix $[A]_n$, which correspond to the eigenvectors $\vec{q}_l$ as well. Similarly, the drift matrix is transformed by applying the relation

$$[Q]_n^{-1} \cdot [B]_n \cdot [Q]_n = [\Gamma]_n. \qquad (17)$$

introducing the matrix $[\Gamma]_n$. Accordingly, the following transformations

$$\vec{\rho}(r) = [Q]_n \cdot \vec{\rho}'(r) \text{ and } \vec{\rho}'(r) = [Q]_n^{-1} \cdot \vec{\rho}(r) \qquad (18)$$

are defined. By multiplying both sides of (14) with $[Q]_n^{-1}$ and using the relations in (16)–(18), the fundamental equation in the transformed domain will result in

$$\frac{\partial}{\partial r}\vec{\rho}'(r) = [\Gamma]_n' \cdot \vec{\rho}'(r) \quad \text{with} \quad [\Gamma]_n' = [\Lambda]_n^{-1} \cdot [\Gamma]_n. \qquad (19)$$

Next, the solution of (19) is examined for each local cell n. The eigenvalues of the matrix $[A]_n$ are complex and include an imaginary part, only, which is either positive or negative as will be shown in the Section II-D. The positive imaginary values correspond to inflow waves and the negative imaginary values correspond to outflow waves, respectively. Hence, these equations can be elucidated as wave equations. Therefore, inflow and outflow boundary conditions in r-direction can be formulated. The formal solution of the differential equation (19) can be written as

$$\vec{\rho}'_{n+1} = \exp([\Gamma]_n' \cdot \Delta r) \cdot \vec{\rho}'_n, \qquad (20)$$

where $\vec{\rho}'_n$ is the initial vector at one edge of the cell n under consideration and Δr is the propagation step that coincides with the discretization width in r-space. $\vec{\rho}'_{n+1}$ is the corresponding

vector at the other edge of the cell n. The exponential operator can also be expressed as [13]

$$\exp\left(-[\Gamma]_n' \cdot \frac{\Delta r}{2}\right) \cdot \vec{\rho}'_{n+1} = \exp\left(+[\Gamma]_n' \cdot \frac{\Delta r}{2}\right) \cdot \vec{\rho}'_n. \qquad (21)$$

For simplicity, the matrix exponential function is approximated by a first order Taylor expansion. In combination with a multiplication of the matrix $[\Lambda]_n$ on both sides of (21) and using (19), we arrive at the following expression

$$\left([\Lambda]_n - [\Gamma]_n \cdot \frac{\Delta r}{2}\right) \cdot \vec{\rho}'_{n+1} = \left([\Lambda]_n + [\Gamma]_n \cdot \frac{\Delta r}{2}\right) \cdot \vec{\rho}'_n. \qquad (22)$$

This is the formal procedure to derive a matrix-vector equation for each cell n.

D. Definition of Self-Energies in r'-Direction

Now, we take a closer look onto the introduced self-energies $\Sigma_{n,1}$ and $\Sigma_{n,L'}$ as well as the eigenvectors with its corresponding eigenvalues according to (15) and (16), respectively. If we assume a negligible correlation between different states at the boundaries 2 (Fig. 1), then the self-energies $\Sigma_{n,1}$ and $\Sigma_{n,L'}$ can be neglected and can be set to zero. This assumption coincides with the idea to apply Dirichlet boundary conditions with $\rho_0(r) = \rho_{L'+1}(r) = 0$. As the matrix $[A]$ is a tridiagonal Toeplitz matrix, the eigenvectors $\vec{q}_l$ of the matrix $[A]_n$ and their components $q_{l,j}$ can be analytically calculated by using the following relation [21]

$$q_{l,j} = i^{j/2} \cdot \sin\left(\frac{j\pi L'}{L'+1}\right) \qquad (23)$$

with $l = j \in 1, 2, \dots, L'$. The corresponding eigenvalues λ_l can be calculated analytically by using the expression [21]

$$\lambda_l = 2 \cdot i \cdot \cos\left(\frac{l \cdot \pi}{L'+1}\right). \qquad (24)$$

Alternatively, the concept of the Wigner-Weyl transform can be applied to define the self-energies. In this case, the solution of the density matrix can be expanded into plane waves. Then, the components $q_{l,j}$ of the eigenvectors $\vec{q}_l$ are given by

$$q_{l,j} = \exp(i \cdot j \cdot k_l \cdot \Delta r) \qquad (25)$$

with $l = j \in 1, 2, \dots, L'$, $\Delta k = \pi/L$ and $k_l = (l - \frac{L'-1}{2}) \cdot \Delta k$. L is the length of the device. The corresponding eigenvalues are given by

$$\lambda_l = 2 \cdot i \cdot \sin(k_l \cdot \Delta r') = 2 \cdot i \cdot \sin\left(\frac{l \cdot \pi}{L'}\right). \qquad (26)$$

In this case the self-energies can be defined by

$$\Sigma_{n,1} = \exp\left(-i \cdot l \cdot \Delta k \cdot \Delta r'\right) \qquad (27)$$

and

$$\Sigma_{n,L'} = \exp\left(+i \cdot l \cdot \Delta k \cdot \Delta r'\right). \qquad (28)$$

For both cases the eigenvectors $\vec{q}_l$ are orthogonal to each other within the interval $-L/2$ and $+L/2$. As both approaches lead to similar results, the results for the latter case are shown further on.

A relation between the proposed approach and the conventional Wigner-Weyl transform can be established, if the expansion based on the eigenvectors (25) is inserted into (5) and if the discretization width $\Delta r'$ is kept small so that the condition $k_l \cdot \Delta r' \ll 1$ holds. Hence, (5) can be rearranged as follows considering the eigenvector $\vec{q}_l$

$$\frac{\partial}{\partial r'}\rho \cong \frac{i \cdot \sin(k_l \cdot \Delta r')}{\Delta r'}\rho_l'(r) \cong i \cdot k_l \cdot \rho_l'(r), \quad (29)$$

because the approximation $\sin(k_l \cdot \Delta r') \cong k_l \cdot \Delta r'$ can be utilized. The result obtained is the approximant when applying the Wigner-Weyl transform onto the corresponding derivative in the r'-domain. The value $\rho_l'(r)$ represents the expansion coefficient with regard to the eigenvector $\vec{q}_l$ and is related to the discretized value $f(k_l, r)$ in the phase space, whereby $f(k, r)$ represents the Wigner function. Finally, from (29) can be concluded that the characteristics of the Wigner-Weyl transform can be formally preserved by the proposed approach.

E. System Matrix and Definition of Self-Energies in r-Direction

The next step addresses the derivation of the system matrix. For this purpose, the matrices $[\delta]_n$ and $[\gamma]_n$

$$[\delta]_n = \left([\Lambda]_n + [\Gamma]_n \cdot \frac{\Delta r}{2}\right) \quad (30)$$

and

$$[\gamma]_n = \left([\Lambda]_n - [\Gamma]_n \cdot \frac{\Delta r}{2}\right) \quad (31)$$

with $n = 1, 2, \ldots, N$ for each cell n are introduced. The matrices $[\delta]_n$ and $[\gamma]_n$ have the matrix dimension of $L' \times L'$. The summation of all the matrix-vector equations with regard to all cells n and with respect to (22) leads to a system matrix $[\mathcal{L}]$ with

$$[\mathcal{L}] = \begin{bmatrix} -[\delta]_1 & [\gamma]_1 & 0 & 0 & 0 \\ 0 & -[\delta]_2 & [\gamma]_2 & 0 & 0 \\ \vdots & \ddots & \ddots & \ddots & \vdots \\ 0 & 0 & -[\delta]_{N-1} & [\gamma]_{N-1} & 0 \\ 0 & 0 & 0 & -[\delta]_N & [\gamma]_N \end{bmatrix}. \quad (32)$$

The system matrix $[\mathcal{L}]$ has a matrix dimension of $L' \cdot N \times L' \cdot (N+1)$. The matrix-vector equation (22) with respect to the first cell $n = 1$ and the last cell $n = N$ needs to be rearranged in order to incorporate boundary conditions at the boundaries 1 in r-direction (Fig. 1). In principle, we follow the descriptive derivation in [13], which allows the combination of non-local characteristics of the drift operator with open boundary conditions. Fermi-Dirac distributions in the phase space dependent k are applied at both boundaries 1. The corresponding distributions in r-space are determined by applying a Fourier transform to the Fermi-Dirac distribution function. Firstly, the relations are defined for the first cell with $r = r_1$. The Fermi-Dirac distribution function at this location is given by

$$f(r_1) = \frac{mk_BT}{2\pi\hbar^2}\ln\left[1 + \exp\left\{\frac{-1}{k_BT}\left(\frac{\hbar^2 k^2}{2m} - \mu\right)\right\}\right]. \quad (33)$$

Hereby, μ is the chemical potential. By taking a discrete Fourier transformation of (33) and exploiting the characteristic that the distribution function f is an even function with respect to k, the distribution function F in the r-space can be calculated according to

$$F(r_1, r_j') = \frac{1}{2\pi}\sum_{k_l} f(k_l) \cdot \cos(k_l \cdot r_j') \cdot \Delta k \quad (34)$$

with $\Delta k = (\pi/L') \cdot \Delta r$. The resulting vector $\vec{F}(r_1)$ is discretized and expanded dependent on the eigenvectors $\vec{q}_l$. With this technique the expansion coefficients c_l' for inflow and outflow waves forming the vector ρ' can be calculated as

$$\vec{\rho'}(r_1) = [Q]^{-1} \cdot \vec{F}. \quad (35)$$

The vector $\vec{\rho'}$ can be separated into two vectors representing the inflow wave vector $\vec{S_1'}(r_1)$ and the outflow wave vector $\vec{S_2'}(r_1)$. With this methodology, the matrix $[\delta]_1$ of the order $L' \times L'$ is splitted into the matrix $[\zeta]_1$ having the matrix dimension of $L' \times L'/2$ with regard to the vector $\vec{S_1'}(r_1)$ and the matrix $[\eta]_1$ with regard to the vector $\vec{S_2'}(r_1)$ having the same matrix dimension as $[\zeta]_1$. So the relation

$$[\delta]_1 = \big[\,[\zeta]_1, [\eta]_1\,\big] \quad (36)$$

is valid. The inflow boundary vector $\vec{S_1'}(r_1)$ can be defined as

$$\vec{S_1'}(r_1) = [\zeta]_1 \cdot \vec{\rho'}(r_1). \quad (37)$$

and can be interpreted as a source vector. Accordingly, the same procedure can be applied for the location $r = r_N$. The matrix $[\gamma]_N$ for the last cell $n = N$ is splitted into the matrix $[\eta]_N$ with regard to the inflow vector $\vec{S_1'}(r_N)$ and the matrix $[\zeta]_N$ with regard to the outflow vector $\vec{S_2'}(r_N)$. Hence, we arrive at

$$[\gamma]_N = \big[\,[\eta]_N, [\zeta]_N\,\big]. \quad (38)$$

The matrix $[\gamma]_N$ has the same dimension as $[\delta]_1$ and the matrices $[\eta]_N$ as well as $[\zeta]_N$ have the same dimension as the matrices $[\eta]_1$ or $[\zeta]_1$. In this case, the outflow vector $\vec{S_2'}(r_N)$ in r-space can be formulated according to

$$\vec{S_2'}(r_N) = [\zeta]_N \cdot \vec{\rho'}(r_{N+1}). \quad (39)$$

Both matrices $-[\eta]_1$ and $[\eta]_N$ are related to the self-energies in r-direction and can be replaced by the self-energy matrices $[\Sigma_1]$ and $[\Sigma_N]$, respectively. By using (36)–(39), the order of the system matrix $[\mathcal{L}]$ in (32) is reduced to a quadratic matrix $[\mathcal{L}']$ of the order $(L' \times N) \times (L' \times N)$ and is of the form

$$[\mathcal{L}'] = \begin{bmatrix} [\Sigma_1] & [\gamma]_1 & 0 & 0 & 0 \\ 0 & -[\delta]_2 & [\gamma]_2 & 0 & 0 \\ \vdots & \ddots & \ddots & \ddots & \vdots \\ 0 & 0 & -[\delta]_{N-1} & [\gamma]_{N-1} & 0 \\ 0 & 0 & 0 & -[\delta]_N & [\Sigma_N] \end{bmatrix}. \quad (40)$$

Furthermore, the boundary vector acting as a source can be defined as

$$\vec{S}' = \left(\vec{S}'_1(r_1), 0, \ldots, 0, -\vec{S}'_2(r_N) \right)^T. \tag{41}$$

Consequently, the following linear matrix-vector equation

$$[\mathcal{L}'] \cdot \vec{\rho}' = \vec{S}' \tag{42}$$

has to be solved. The vector $\vec{\rho}'$ has to be transformed back by using the transformation (18) for each cell n to get the density matrix $\vec{\rho}$ in the original space (r, r'). Formally, (42) can be rearranged in a way so that between contributions from self-energies in r-direction and from the Liouville operator can be differed. The matrix $[\mathcal{L}']$ can be simply defined by $[\mathcal{L}'] = [\mathcal{L}_0] - [\Sigma]$, in which the matrix $[\Sigma]$ contains the matrices $[\Sigma_1]$ and $[\Sigma_N]$ representing outflowing characteristics. This interpretation leads to the representation

$$([\mathcal{L}_0] - [\Sigma]) \cdot \vec{\rho}' = \vec{S}'. \tag{43}$$

Following the self-energy concept, the vector $\vec{S}'$ describes incoming or source waves. Note, the matrix $\mathcal{L}_0$ still considers the self-energy concept in r'-direction.

III. SELF-CONSISTENT CALCULATION

In this section, the procedure to solve the transport equation along with the Poisson equation self-consistently is described briefly. For a spatially constant dielectric permittivity of the medium, the Poisson equation reads as

$$\frac{d}{dr} \varepsilon(r) \frac{d}{dr} V(r) = e \cdot [\rho(r, r')|_{r'=0} - N_d(r)], \tag{44}$$

where $\varepsilon(r) = \varepsilon_0 \cdot \varepsilon_r(r)$ represents the static dielectric permittivity of the medium, $V(r)$ is the potential, $\rho(r, r')|_{r'=0}$ is the electron carrier density calculated from the real part of the statistical density matrix $\rho(r, r')$ and $N_d(r)$ represents the doping profile, respectively. The Gummel method [22] is applied iteratively for the self-consistent solution of the Liouville-von Neumann-Poisson-equation system. The Gummel method described in [23] and the discretization scheme for the Poisson equation therein are applied. Furthermore, the convergence error χ with regard to the iterative solution is calculated according to the following relation by applying a quadratic norm [24]

$$\| V_{j+1} - V_j \|_2 \leq \chi \cdot \| V_{j+1} \|_2, \tag{45}$$

where j denotes the number of iteration steps. Throughout our calculations, a convergence error of 10^{-3} has been chosen by terminating the iteration procedure and defining the approximated self-consistent solution. If this aspect would have not been addressed properly, an oscillation pattern could have been observed from the results obtained.

IV. EXAMPLES

To validate the effectiveness of the proposed method, a resonant tunneling diode (RTD) is introduced as a prototype device. The structure and the parameters of the conduction band for this particular device under consideration are given in Fig. 2. A constant effective mass is assumed over the whole length of the
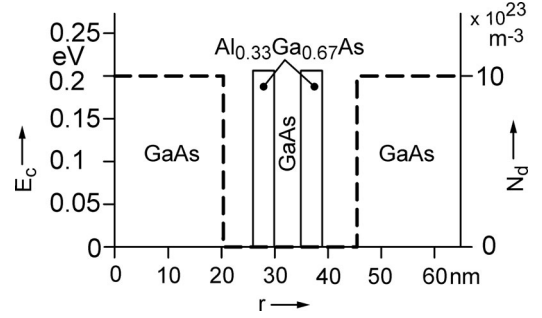

Fig. 2. The conduction band E_c of the RTD under investigation. The 66 nm wide structure consists of two 5 nm wide $Al_{0.33}Ga_{0.67}As$ potential barrier layers and a 6 nm wide GaAs quantum well (solid line). The distribution of the doping concentration N_d is also shown (dashed line).

device with $m = 0.063 m_0$. The chemical potential μ is set to be 0.04617 eV at both sides of the device when considering a spatial behavior of the doping concentration according to Fig. 2. For calculation purposes, the numbers of discretization points are chosen to be $L' = 1000$ and $N = 67$. The discretization widths are set to be $\Delta r = 1$nm and $\Delta r' = 2$ nm.

To evaluate the results obtained by utilizing the proposed approach, the results are compared with those stemming from the quantum transmitting boundary method (QTBM) [2] and from the solution of the conventional Wigner transport equation by applying a second order upwind difference scheme (UDS2) [8]. The resulting Wigner function in the (r, k)-space is calculated and transformed into the (r, r')-space using the inverse Wigner-Weyl transform. For the purpose of an efficient comparison, the values of the statistical density matrix in the (r, r')-space are shown, only. Especially, the QTBM can be used as a reference method, because it is an equivalent but numerical representation of the non-equilibrium Green's function method [25], [26] and considers self-energies. When applying the QTBM approach, an analytical integration in k-space is utilized to determine the solution. So accurate results are obtained from the Schrödinger based numerical solutions. The number of discretization points and the discretization width in r-direction are chosen in the same manner as in the proposed method. For the choice of discretization points of $L' = 250$ and $L' = 500$ in r'-direction, the solutions are comparable with the solutions obtained by the QTBM, but final convergence is achieved for $L' = 1000$. The large number for L' is reasonable because the r'-space corresponds to the k-space and a dense discretization in r'-space is neccessary to obtain comparable results with the analytical solution when applying the QTBM. Note, in contrast to the QTBM, the solution of (43) can be determined in one step avoiding the repeated solution of Schrödinger equation as well as the time-consuming analytical integration in k-space. Of course, the order of the matrix is by a factor of L' larger than in the case of the QTBM, but (43) can be efficiently solved as sparse matrices showing a block diagonal structure occur. Finally, in this work the calculation time has been by a factor of 2 up to 3 order smaller than from the QTBM. Of course, the calculation time can be further reduced by more effective numerical methods, but related investigations are beyond the scope of this work. Additionally, the proposed approach is modified in a way

that a UDS2 is applied onto (13). A finite difference scheme according to

$$\frac{\partial \rho'}{\partial r} \cong \frac{1}{2\Delta r} \cdot \begin{cases} -\rho'_{j,n+1} + 4\rho'_{j,n+1} - 3\rho'_{j,n} & \lambda_{\mathrm{imag},j} \leq 0 \\ +\rho'_{j,n-2} - 4\rho'_{j,n-1} + 3\rho'_{j,n} & \lambda_{\mathrm{imag},j} > 0. \end{cases} \tag{46}$$

is applied at each location $r = r_n$ and for each imaginary part $\lambda_{\mathrm{imag},j}$ of the eigenvalue λ_j. The methodology to solve the whole system of matrix equations corresponds to the solution of the discretized Wigner transport equation, so we refer to [13] for further details. This allows an in depth comparison with the conventional Wigner approach [9], [13]. The main difference between both approaches is the use of a different basis, as on the one hand the basis is defined by Fourier exponentials and on the other hand a basis is defined by the eigenvectors of a Toeplitz matrix as given in (23) or (25). All mentioned methods are compared with each other with regard to the real and imaginary parts of the density matrices, carrier densities and current densities. A thermal equilibrium case and self-consistent non-equilibrium cases for external applied voltages of $U_e = |0.1\,\mathrm{V}$ and $U_e = 0.3\,\mathrm{V}$ are investigated. Furthermore, a steady state I-V curve is computed for the non-equilibrium case. Sections are organized in the following way: Section IV-A describes the results related to the case of a thermal equilibrium whereas the results regarding the case of a self-consistent non-equilibrium are discussed in Section IV-B followed by the presentation of a steady state I-V-curve.

A. Thermal Equilibrium Case

The density matrices under thermal equilibrium are calculated for all the enumerated methods and are shown in Fig. 3. The real parts of the density matrices calculated by applying the proposed method and the QTBM are shown in Fig. 3(a) and (b), while the density matrices computed by using the second order upwind difference scheme for the proposed approach and for the Wigner transport equation are shown in Fig. 3(c) and (d). In theory, the values of the imaginary part of the density matrix should be zero. The values of the imaginary parts of both, the proposed method and QTBM, are of the order eight up to nine smaller than the magnitude of the real parts, so the corresponding imaginary parts are negligible in comparison to their real counterparts. On the other hand, the imaginary parts of both UDS2 are only of the order one up to two smaller than the magnitude of their real counterparts. As the magnitude is at least one or two orders smaller, the imaginary parts are not negligible and are shown in Fig. 4(a) and (b), respectively. From Fig. 3, it can be observed that the results of the proposed method and the QTBM agree with each other quite well. A negligible correlation between different states appears for both methods for large values of r' (Fig. 3(a) and (b)), while a significant correlation between different states at the cross diagonals can be observed for the methods utilizing the upwind difference scheme (Fig. 3(c) and (d)). The values of the imaginary parts of the corresponding density matrices exhibit a similar interference pattern. Additionally, a strong deviation from zero can be observed along and near the $r' = 0$-axis. This leads to errors as
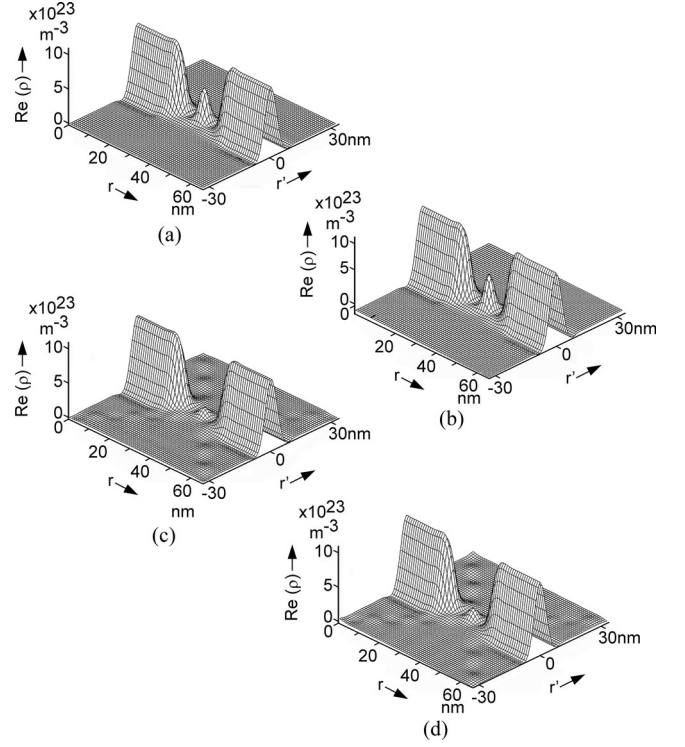

Fig. 3.   Real parts of the density matrices under thermal equilibrium: (a) Proposed Method, (b) QTBM, (c) UDS2 in (r, r')-space, (d) Density Matrix calculated from the Wigner distribution function using the UDS2 in (r, k) space.
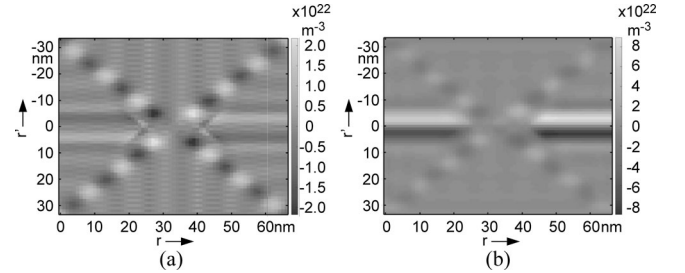

Fig. 4.   Imaginary parts of the density matrices under thermal equilibrium: (a) UDS2 in (r, r') space, (b) Density Matrix calculated from the Wigner distribution function using the UDS2 in (r, k) space.

discussed above. The current density is calculated dependent on the r-coordinate by using the relation

$$J(r) = \frac{e \cdot \hbar}{m} \cdot \mathrm{Im} \left(\frac{\partial}{\partial r'} \left\{ \rho(r, r')|_{r'=0} \right\} \right). \tag{47}$$

Here, $J(r)$ represents the current density. The current density must be zero at all locations along the device, when the case of a thermal equilibrium is investigated and scattering effects are not incorporated. The current density for the proposed method and the QTBM are close to zero within the numerical accuracy. Instead, the current density for both versions of UDS2 is non-zero and varies along the r-coordinate. This error is a result of the described deviations with regard to $\rho(r, r')$ close to the $r' = 0$-axis. The basic reason for the existence of these interference effects and the deviations along and in the vicinity of the $r' = 0$-axis is a result of the fact that the diffusion effects are
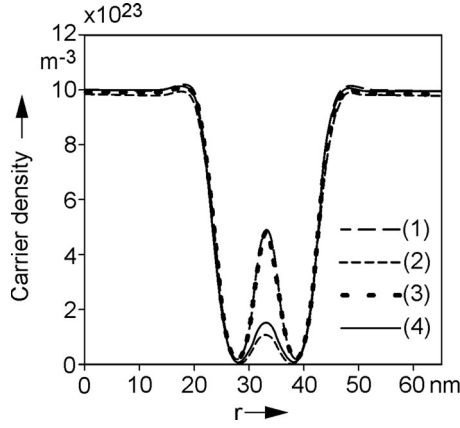
Fig. 5. Carrier density for (1) the QTBM, (2) the Wigner-Weyl transform, (3) the proposed approach with a trapezodial scheme and (4) a UDS2.

overestimated when applying the upwind difference scheme [9]. If this overestimation is avoided and if the non-local drift operator is approximated adequately [13], as it has been done here analogously, the unphysical interference pattern can be avoided. This non-local mechanism is also inherently included within the QTBM. Next, the carrier density for $n(r)$ is calculated by using the relation

$$n(r) = \rho(r, r')|_{r'=0}. \tag{48}$$

The carrier density $n(r)$ is calculated and shown in Fig. 5. It can be observed from Fig. 5 that the carrier density $n(r)$ between the barriers and within the barriers differs significantly. The values of the proposed method agree very well with the values obtained by applying the QTBM, which justifies the effectiveness of the proposed approach. The results based on the methods utilizing the UDS2 deviate strongly from the results obtained from both other methods. As discussed, the overestimation of diffusion effects causes the unphysical interference pattern and explains the deviations in Fig. 5. The spatial behavior of the eigenstates and its corresponding error at $r = L/2$ correlates with the spatial behavior of the eigenstates at each location r. Therefore, the unphysical interference pattern appears at the cross diagonals as can be seen from Figs. 3 and 4.

B. Non-Equilibrium Case

The density matrices for the non-equilibrium case are calculated under consideration of the Poisson equation as described in Section III. As examples, the external voltages of $U_e = 0.1$ V and $U_e = 0.3$ V are applied. At first, the case of $U_e = 0.1$ V is investigated. The real parts of the density matrices calculated are shown in Fig. 6(a) for all methods while their imaginary parts are shown in Fig. 7(a). Additionally, the carrier density is calculated for all the enumerated methods using (48) and depicted in Fig. 8. From Figs. 6(a), 7(a), and 8, it can be concluded that, once again, the results from the proposed method agree very well with the results obtained from the QTBM. The results based on the methods utilizing the UDS2 deviate strongly from the proposed approach and the QTBM. Also, this particular statement holds for the carrier density between the barriers and within the barriers, which differs from the proposed ap-
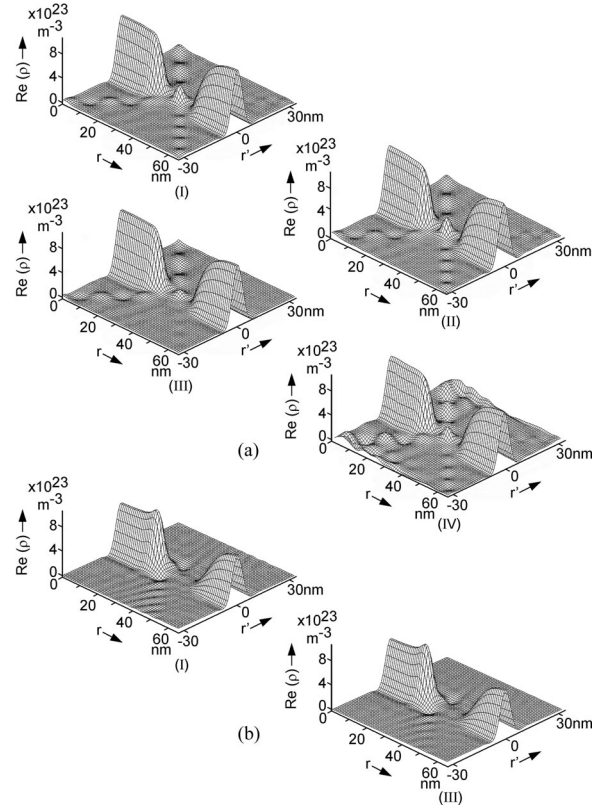

Fig. 6. Real parts of the density matrices (a) for $U_e = 0.1$ V and (b) for $U_e = 0.3$ V: (I) Proposed Method, (II) QTBM, (III) UDS2 in (r, r') space, (IV) Density Matrix calculated from the Wigner distribution function using the UDS2 in (r, k) space.

proach and the QTBM (Fig. 8). Due to the different gradients of the carrier densities within the barriers, the interaction of the overestimated diffusion current and drift current is different. An asymmetric interference pattern is expected. This asymmetric behavior of the coherence patterns can be confirmed by the results shown in Fig. 6(a) as well as Fig. 7(a). The coherence effect is significantly lower for values with $r > L/2$ in comparison to the values with $r < L/2$. Another interesting aspect can be observed from Fig. 6(d). The solution for the Wigner transport equation differs from the other methods for values of r close to zero. The difference originates from an aliasing effect, which is inherently linked with the Wigner-Weyl transform [14]. This aliasing effect results in a strong coherence pattern for values of r close to zero. The aliasing effect can be reduced by choosing a larger computational window. Of course, this results in a significant decrease of the computational efficiency. Secondly, real and imaginary parts of the density matrices calculated under $U_e = 0.3$V are shown in Figs. 6(b) and 7(b), respectively. The carrier density is depicted in Fig. 8. While the deviations with regard to the imaginary parts of the density matrices are considerably high, the deviations with regard to their real counterparts are smaller. Therefore, only the real parts are shown for the proposed approach and the UDS2 approach in the (r, r') space. The same conclusions can be drawn even for the case of $U_e = 0.3$ V. For completeness, the position dependent current density and the potential profile of externally applied voltages are shown in Fig. 9. In case the effective mass is assumed to be
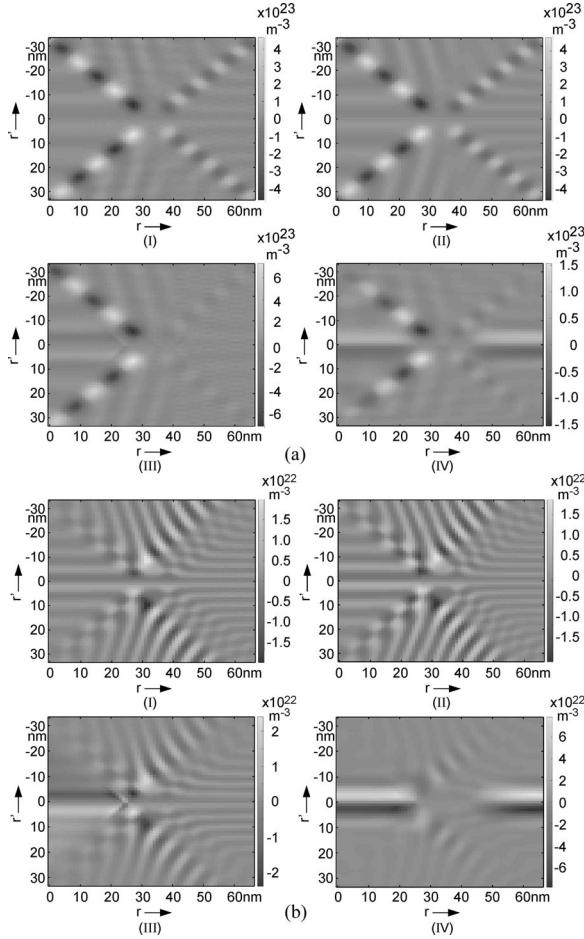
Fig. 7.   Imaginary parts of the density matrices (a) for $U_e = 0.1$ V and (b) for $U_e = 0.3$ V: (I) Proposed Method, (II) QTBM, (III) UDS2 in (r, r') space, (IV) Density Matrix calculated from the Wigner distribution function using the UDS2 in (r, k) space.
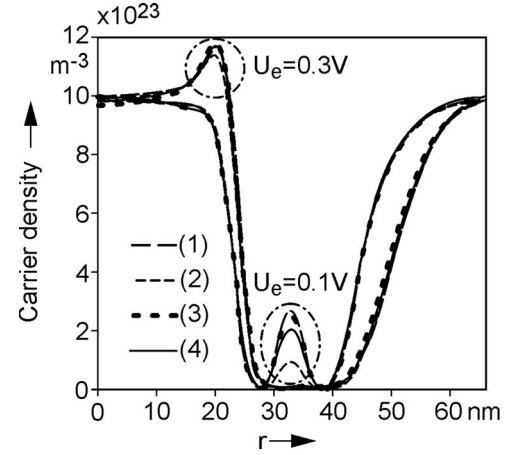

Fig. 8.   Carrier density for $U_e = 0.1$ V and $U_e = 0.3$ V by using (1) the QTBM, (2) the Wigner-Weyl transform, (3) the proposed approach with a trapezodial scheme and (4) a UDS2.
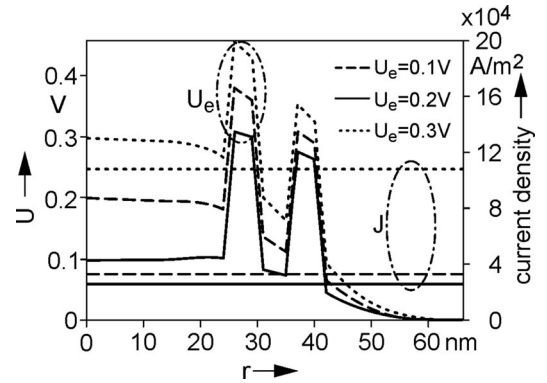

Fig. 9.   Position dependent current density $J(r)$ and potential $U(r)$ for different externally applied voltages U_e at: (1) 0.1 V, (2) 0.2 V and (3) 0.3 V.
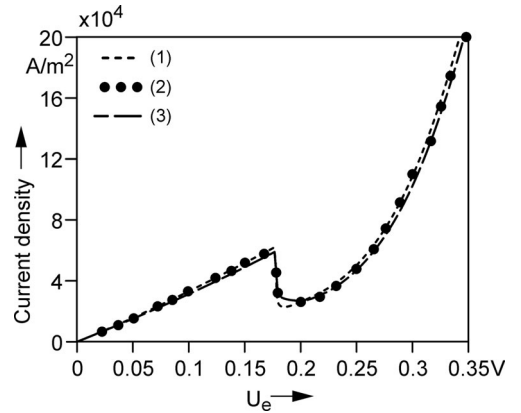

Fig. 10.   Steady state I-V curves are shown applying (1) the QTBM, (2) the proposed approach with a trapezodial scheme and (3) the UDS2. The current density is shown dependent on the applied voltage U_e.

constant across the entire device, the wave function as a solution of Schrödinger's equation and its derivative at the interfaces are continous resulting in a spatially constant current density $J(r)$. Therefore, the continuity equation is fullfilled and because scattering is not considered, the current density $J(r)$ should be constant along the device. As can be seen from Fig. 9, the spatially calculated current density $J(r)$ is constant as it is postulated. The steady state I-V curve is computed for the proposed method, the QTBM and the UDS2 by using (47). The results are shown in Fig. 10. The range of the applied voltage is varied from 0 V up to 0.35 V. The steady state I-V characteristics curve obtained from the proposed method shows an excellent agreement with the results obtained from the QTBM. Particular attention has to be drawn to the convergence of the final results obtained. The voltage peak V_p at resonance is about 0.172 V. This value can be estimated by the energy eigenvalue of the resonant state for the non-selfconsistent case, which is determined to be $E_0 = 0.0625$ eV. The estimated minimum peak value given by $V_p = 2 \cdot E_0/e = 0.125$ V is, of course, smaller than the actual peak value as the self-consistent case has been considered.

V. DISCUSSION AND CONCLUSION

From the numerical point of view, the use of the Wigner-Weyl transform can be a source for a few serious problems. The origin of these problems results from the convolution, which appears, after the Wigner-Weyl transform is applied onto (4).

One essential prerequisite to evaluate the convolution is that the Wigner-Weyl transform of the drift term must exist and, therefore, requires the integrability of the drift term. This assumes that the values for $V(r \to \infty)$ and $V(r \to -\infty)$ converge to zero. With respect to modelling purposes this is the case for the equilibrium case independent whether a self-consistent solution along with the incorporation of the Poisson equation is considered or not. In case external voltages are applied, this condition cannot be fulfilled in general. Finally, the integrability cannot be obtained. The use of a discrete Fourier transform and its application onto the drift term leads to a suitable approximation, only, if high spatial frequencies are considered in the Fourier series. The latter aspect results in a bad convergence of the solution and, therefore, is linked with numerical problems.

Along with the presented method, these problems can be avoided. The discretization and the eigenvector basis can be chosen in a way that the device under investigation can be numerically fully described within the defined computational window. Furthermore, the characteristics of the Wigner-Weyl transform can be reflected by the choice of eigenvectors. Open boundary conditions with their corresponding self-energy terms can be considered reflecting the nature of nonlocal quantum mechanics. With the presented approach the solution of the Liouville-von Neumann equation can be combined with the advantages of conventional non-equilibrium Green's function approaches. Additionally, the Liouville-von Neumann equation is part of the Kossakowski-Lindblad equation, which not only allows the inclusion of coherent effects but also the description of incoherent effects. As an advantage, in contrast to the conventional QTBM, the proposed approach offers the possibility to be extended to include coherent and incoherent transport effects on a transient basis.

REFERENCES

[1] J. P. Sun, G. I. Haddad, P. Mazumder, and J. N. Schulman, "Resonant tunneling diodes: Models and properties," *Proc. IEEE*, vol. 86, no. 4, pp. 641–661, Apr. 1998.

[2] C. S. Lent and D. J. Kirkner, "The quantum transmitting boundary method," *J. Appl. Phys.*, vol. 67, no. 10, pp. 6653–6359, 1990.

[3] P. Douglas Yoder, M. Grupen, and R. Kent Smith, "Demonstration of intrinsic tristability in double-barrier resonant tunneling diodes with the Wigner transport equation," *IEEE Trans. Electron Devices*, vol. 57, no. 12, pp. 3265–3274, Dec. 2010.

[4] N. C. Kluksdahl, A. M. Kriman, D. K. Ferry, and C. Ringhofer, "Self-consistent study of the resonant-tunneling diode," *Phys. Rev. B*, vol. 39, pp. 7720–7735, 1989.

[5] E. Wigner, "On the quantum correction for thermodynamic equilibrium," *Phys. Rev.*, vol. 40, no. 5, pp. 749–759, 1932.

[6] P. Vogl and T. Kubis, "The non-equilibrium Green's function method: An introduction," *J. Comput. Electron*, vol. 9, no. 3, pp. 237–242, 2010.

[7] O. Baumgartner, P. Schwaha, M. Karner, M. Nedjalkov, and S. Selberherr, "Coupling of non-equilibrium Green's function and Wigner approaches," *Proc. IEEE, Int. Conf. Simul. Semicond. Processes Devices*, 2008, pp. 345–348.

[8] K. Y. Kim and B. Lee, "Simulation of quantum transport by applying second-order differencing scheme to Wigner function model including spatially varying effective mass," *Solid State Electron.*, vol. 43, no. 1, pp. 81–86, 1999.

[9] W. R. Frensley, "Wigner function model of a resonant-tunneling semiconductor device," *Phys. Rev. B*, vol. 36, no. 3, pp. 1570–1580, 1987.

[10] K. K. Gullapalli, D. R. Miller, and D. P. Neikirk, "Simulation of quantum transport in memory-switching double-barrier quantum-well diodes," *Phys. Rev. B*, vol. 49, no. 4, pp. 2622–2628, Jan. 1994.

[11] R. Courant, E. Isaacson, and M. Rees, "On the solution of nonlinear hyperbolic differential equations by finite differences," *Commun. Pure Appl. Math.*, vol. 5, no. 3, pp. 243–255, 1952.

[12] R. Rosati, F. Dolcini, R. C. Iotti, and F. Rossi, "Wigner function formalism applied to semiconductor quantum devices: Failure of the conventional boundary condition scheme," *Phys. Rev. B*, vol. 88, no. 3, pp. 3451–3466, 2013.

[13] D. Schulz and A. Mahmood, "Approximation of a phase space operator for the numerical solution of the Wigner transport equation," *IEEE J. Quantum Electron.*, vol. 52, no. 2, Feb. 2016, Art. no. 8700109.

[14] T. Classen and W. Mecklenbrauker, "The aliasing problem in discrete-time Wigner distributions," *IEEE Trans. Acoust., Speech, Signal Process.* vol. ASSP-31, no. 05, pp. 1067–1072, Oct. 1983.

[15] H. Mizuta and C. J. Goodings, "Transient quantum transport simulation based on statistical density matrix," *J. Phys.* vol. 3, no. 21, pp. 3739–3756, 1991.

[16] T. L. Beck, "Real-space mesh techniques in density-functional theory," *Rev. Mod Phys.*, vol. 72, no. 4, pp. 1074–1080, 2000.

[17] W. R. Frensley, "Simulation of resonant tunneling heterostructure devices," *J. Vac. Sci. Technol. B*, vol. 3, no. 4, pp. 1261–1266, 1985.

[18] L. Schulz and D. Schulz, "Application of a slowly varying envelope function onto the analysis of the Wigner transport equation," *IEEE Trans. Nanotechnol.* vol. 15, no. 5, pp. 801–809, Sep. 2016.

[19] E. Polizzi and S. Datta, "Multidimensional nanoscale device modeling: The finite element method applied to the non-equilibrium Green's function formalism," in *Proc. 3rd IEEE Conf. Nanotechnol.*, 2003, pp. 40–43.

[20] S. Datta, "Nanoscale device modeling: The Green's function method," *Superlattices Microstruct.*, vol. 28, no. 4, pp. 253–278, 2000.

[21] S. Noschese, L. Pasquini, and L. Reichel, "Tridiagonal Toeplitz matrices: Properties and novel applications," *Numer. Linear Algebra Appl.*, vol. 20, no. 2, pp. 302–326, 2013.

[22] H. K. Gummel, "A self-consistent iterative scheme for one-dimensional steady-state transistor calculations," *IEEE Trans. Electron Devices*, vol. 11, no. 10, pp. 455–465, Oct. 1964.

[23] O. Pinaud, "Transient simulations of a resonant tunneling diode," *J. Appl. Phys.*, vol. 92, no. 4, pp. 1987–1994, 2002.

[24] J. F. Mennemann, A. Jüngel, and H. Kosina, "Transient Schrödinger–Poisson simulations of a high-frequency resonant tunneling diode oscillator," *J. Comput. Phys.*, vol. 239, pp. 187–205, 2013.

[25] H. Jiang, S. Shao, W. Cai, and P. Zhang, "Boundary treatments in non-equilibrium Greens function (NEGF) methods for quantum transport in nano-MOSFETs," *J. Comp. Phys.* vol. 227, no. 13, pp. 6553–6573, 2008.

[26] Y. He, T. Kubis, M. Povolotskyi, J. Fonseca, and G. Klimeck, "Quantum transport in NEMO5: Algorithm improvements and high performance implementation," in *Proc. IEEE Int. Conf. Simul. Semicond. Processes Device*, 2014, pp. 361–364.

Khuram Shahzad Khalid was born in Wah Cantt, Pakistan, in 1985. He received the M.Sc. degree in electrical engineering from the University of Engineering and Technology Taxila, Taxila, Pakistan, in 2011. He is currently working toward the Doctorate degree at the Chair of High Frequency Techniques, Technische Universität Dortmund, Dortmund, Germany. From 2007 to 2014, he was a Lecturer and a Lab Engineer at the Wah Engineering College, University of Wah, Wah Cantt, Pakistan. His current research interests include the field of modeling and simulation of terahertz quantum devices.

Lukas Schulz was born in Recklinghausen, Germany, in 1992. He received the B.Sc. degree in electrical engineering and information technology from the Technische Universität Dortmund, Dortmund, Germany, in 2015. He has been a Student Assistant at the Chair of High Frequency Techniques, Technische Universität Dortmund, since 2015. His current research interests include the simulation of quantum devices including coherent and kinetic models.

Dirk Schulz was born in Düsseldorf, Germany, in 1965. He received the Dipl.-Ing. degree in electrical engineering from the RWTH Aachen University, Aachen, Germany, in 1990, and the Dr.-Ing. and Venia Legendi degrees from the Technische Universität Dortmund, Dortmund, Germany, in 1994 and 2001, respectively. He has been a Research Assistant at the Chair of High Frequency Techniques, Technische Universität Dortmund, since 1990. His current research interests include the field of modeling and simulation of photonic and terahertz devices.